Marine Wind and Wave Height Trends at Different ERA-Interim Forecast Ranges

OLE JOHAN AARNES

Norwegian Meteorological Institute, and Geophysical Institute, University of Bergen, Bergen, Norway

SALEH ABDALLA, JEAN-RAYMOND BIDLOT, AND ØYVIND BREIVIK

European Centre for Medium-Range Weather Forecasts, Reading, United Kingdom

ABSTRACT

Trends in marine wind speed and significant wave height are investigated using the global reanalysis ERA-Interim over the period 1979–2012, based on monthly-mean and monthly-maximum data. Besides the traditional reanalysis, the authors include trends obtained at different forecast range, available up to 10 days ahead. Any model biases that are corrected differently over time are likely to introduce spurious trends of variable magnitude. However, at increased forecast range the model tends to relax, being less affected by assimilation. Still, there is a trade-off between removing the impact of data assimilation at longer forecast range and getting a lower level of uncertainty in the predictions at shorter forecast range. Because of the sheer amount of assimilations made in ERA-Interim, directly and indirectly affecting the data, it is difficult, if not impossible, to distinguish effects imposed by all updates. Here, special emphasis is put on the introduction of wave altimeter data in August 1991, the only type of data directly affecting the wave field. From this, it is shown that areas of higher model bias introduce quite different trends depending on forecast range, most apparent in the North Atlantic and eastern tropical Pacific. Results are compared with 23 in situ measurements, *Envisat* altimeter winds, and two stand-alone ECMWF operational wave model (EC-WAM) runs with and without wave altimeter assimilation. Here, the 48-h forecast is suggested to be a better candidate for trend estimates of wave height, mainly due to the step change imposed by altimeter observations. Even though wind speed seems less affected by undesirable step changes, the authors believe that the 24–48-h forecast more effectively filters out any unwanted effects.

1. Introduction

Long-term observation records of marine wind and sea state are scarce in comparison with the time series found over land routinely collected since the nineteenth century in certain populated regions of Earth (Hurrell 1995). The need for long, reliable time series of marine near-surface winds U_{10} and significant wave height H_s is increasing as climate projections require a baseline climatology against which to be compared, and even more so if dynamical models of the sea state are to be included in future coupled climate scenarios (Cavaleri et al. 2012; Dobrynin et al. 2012; Sterl et al. 2012; Hemer et al. 2013; Khon et al. 2014). There are also more immediate needs for reliable time series of past wind and wave climate,

such as estimates of return values in areas without observational records (Caires and Sterl 2005; Aarnes et al. 2012; Breivik et al. 2013, 2014) or decadal trends in wind and wave parameters. A number of recent regional studies on wave climate variability and trends from hindcasts and reanalyses are presented in Appendini et al. (2014) (Gulf of Mexico); Reguero et al. (2013) and Izaguirre et al. (2013) (Central and South America); Bromirski et al. (2013) (North Pacific); Dodet et al. (2010), Bertin et al. (2013), Wang and Swail (2001), and Wang et al. (2012) (North Atlantic); and Wang and Swail (2002) and Semedo et al. (2011) (Northern Hemisphere). Most of these studies are to some extent directly or indirectly affected by data assimilation. Therefore, trend estimates from altimeter wave heights are an attractive alternative; see, for example, Hemer et al. (2010) (Southern Hemisphere) and Young et al. (2011, 2012) (global). These studies, however, rely highly on intercalibration between satellite missions.

Corresponding author address: Ole Johan Aarnes, Norwegian Meteorological Institute, Allégaten 70, NO-5007 Bergen, Norway.
E-mail: ole.aarnes@met.no

Global marine wind and wave reanalyses can be powerful proxies for observational records, provided that they do indeed prove reliable in data-scarce regions and periods. With the advent of long marine Earth-observing satellite missions (European Remote Sensing Satellites *ERS-1* and *ERS-2*, starting in 1991), the quality and coverage of marine U_{10} and H_s observations rose dramatically. Since such observations are usually assimilated into global reanalyses the question of the quality of a reanalysis before and after the satellite era should be addressed.

Numerical weather prediction models are confined by several characteristics, the inherent physics, resolution, and numerics. Parameters such as U_{10} and H_s will vary accordingly. If the modeled wind and wave climate corresponds to the observed climate, assimilation becomes a mere way to keep the model on the right track. Should the model however have an inherent bias relative to the observed climate, data assimilation will force the model away from its own climate, only to revert back as the model is integrated forward in time (forecast) less constrained by assimilation. In this way, a model may end up with different statistics at the time of analysis (hereafter ANA) and at increased forecast range (FCR). Not surprisingly, ANA will correlate better with the real climate, the reason why reanalyses are particularly attractive for studying past climate. However, as the number and quality of assimilations vary with time, it is reasonable to assume ANA to reflect these changes. Any discrepancies found between the model output at ANA and increased FCR may potentially identify any model biases, or equivalently effects of assimilation. In the end, if we are not correcting model bias at ANA, the trend should be similar at ANA and increased FCR, assuming model drift is insignificant.

ERA-Interim (hereafter ERA-I) is a reanalysis developed by the European Centre for Medium-Range Weather Forecasts (ECMWF) under the European Reanalysis Project (ERA), coupling atmosphere and surface waves, covering the period from 1979 to the present day (see Dee et al. 2011). Besides the traditional reanalysis, ERA-I also performs 10-day forecasts from reanalyzed fields twice a day. Since 1979, the number of observations assimilated has increased substantially. Between 1989 and 2010, there was a tenfold increase, from 10^6 to 10^7 day^{-1}, with the biggest addition coming from spaceborne instruments. The only wave data products used in ERA-I are the significant wave height observations from radar altimeters on board the satellites *ERS-1*, *ERS-2*, *Environmental Satellite* (*Envisat*), *Jason-1*, and *Jason-2* available for different periods, but with almost sustained existence since August 1991. Even though the atmospheric model and the wave model are coupled, the wave data analysis is done independently

from the atmospheric assimilation. The wave model assimilation scheme, first developed by Lionello et al. (1992), is based on the optimum interpolation (OI) technique. This simple scheme provides an update to the significant wave height field at ANA that is produced by the coupled system following its four-dimensional variational assimilation of all sort of atmospheric data. This update is then translated into an update of the model spectra used for the subsequent model integration. Ideally, a data assimilation scheme should only correct for random error in the model; otherwise, the model biases would quickly reappear once the model is integrated beyond ANA. This is even more prominent in a forced system such as the wave model with an OI scheme such as that employed in ERA-I.

Since altimeter wave height data originate from several instruments with different characteristics and processing procedures, there is a need for intercalibration to harmonize them. For ERA-I, this was done with respect to in situ observations (J. Bidlot 2015, unpublished manuscript). Considering the fact that the wave-height climate characteristics from in situ observations are not the same as ERA-I model, first, ERA-I wave heights exhibit systematic biases with respect to in situ data (J. Bidlot 2015, unpublished manuscript) and, consequently, biases with respect to the intercalibrated altimeter data (Abdalla et al. 2011). These biases are partially corrected at ANA with the introduction of intercalibrated altimeter data. However, before August 1991 or during periods when altimeter data are temporarily not available, the ERA-I wave heights return to their biased state.

In this study we investigate trends in H_s and U_{10} based on ERA-I and how they are affected by nonstationary assimilation over the period 1979–2012. The aim is to detect any spurious trends and possibly propose an alternative to ANA (i.e., an FCR offering trends more representative of the real climate). Special attention is being made on the era with and without altimeter wave height assimilation. We compare ERA-I with observational records from buoys and satellites, taking care to distinguish between independent datasets and datasets that have been assimilated in the reanalysis. A similar study based on atmospheric temperature from ERA-I may be found in Simmons et al. (2014).

The paper is organized as follows. Section 2 introduces the data [i.e., ERA-I, two stand-alone ECMWF operational wave model (EC-WAM) runs with and without altimeter wave height assimilation] and observations, in situ and altimetry. Section 3 presents the methodology for trend estimation and the RHtestsV4 (Wang and Feng 2013) software package, a homogenization tool used herein to correct for step changes inherent in the in situ observations. Section 4 presents global trends in H_s and U_{10} and

TABLE 1. Altimeter H_s assimilated in ERA-I.

ERS-1	1 Aug 1991–3 Jun 1996
ERS-2	3 May 1995–21 Jul 2003
Envisat	21 Jul 2003–April 2012
Jason-1	20 Oct 2003–3 Jul 2013
Jason-2	1 Feb 2010–present

comparisons between the different datasets. Section 5 discusses the results and relates the findings with similar studies. Finally, section 6 offers some conclusions.

2. Data

a. ERA-Interim

ERA-I presents a third-generation reanalysis at the ECMWF and possess a number of improvements from its predecessors ERA-15 (Gibson et al. 1997) and ERA-40 (Uppala et al. 2005); see Dee et al. (2011) for more information. The ongoing project was originally meant to improve the data-rich period of the 1990s and 2000s following the appearance of Earth-observing satellites such as *ERS-1*. In 2011 the reanalysis was extended backwards from January 1989 to January 1979.

ERA-I is run with the same setup as the Integrated Forecasting System (IFS) release cycle Cy31r2, used operationally at ECMWF during the period December 2006 through June 2007. The horizontal resolution of the atmospheric model is approximately 79 km (T255 spectral truncation) on a reduced Gaussian grid. The coupled wave component (Janssen 2004) is somewhat coarser at approximately 110 km. The wave model is run with shallow water physics where appropriate and discretized using 24 directions and 30 frequencies.

Prior to 2002, most of the observations assimilated in ERA-I are similar to those used in ERA-40 with some improvements [see section 4.1 of Dee et al. (2011) for details]. In the context of this study, the most notable changes were additional and recalibrated scatterometer surface wind speeds, reprocessed wave data from *ERS-1* and *ERS-2* calibrated against buoy data and improved satellite radiance data. After 2002, ERA-I uses observations from the ECMWF's operational archive. ERA-I assimilates altimeter H_s data (see Table 1) and buoy U_{10} data, while in situ H_s and altimeter U_{10} are not used in the reanalysis and can serve to independently evaluate the merits of the reanalyses.

ERA-I is run twice daily, at 0000 and 1200 UTC, but offers 6-hourly data at ANA, a blend of analysis and 6-hourly reforecasts. Beyond the 12-h FCR, reforecasts are only available at 0000 and 1200 UTC. To be consistent, we have calculated monthly means and monthly maxima at ANA and increased FCR based on 0000 and 1200 UTC only.
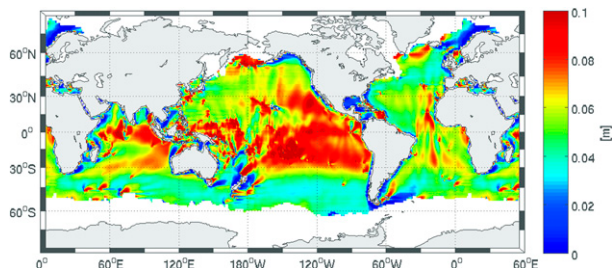

FIG. 1. Mean discrepancy in H_s between ERA-I (ANA) and WAM-AS over the period 1992–2011.

b. EC-WAM run with and without altimeter wave height assimilation

In the following we compare two stand-alone EC-WAM runs with and without wave altimeter assimilation (hereafter denoted as WAM-AS and WAM-NAS, respectively), that are otherwise identical. Both runs are forced with archived ERA-I winds equivalent to U_{10}^{ANA} and span the period 1992–2011 (20 yr). While ERA-I uses a 30-min time step and evolving wind fields, the wind fields forcing the stand-alone runs are sampled every 6 h and kept constant over the same period. Unlike ERA-I, which is run with two-way interaction, the wave model is run in a separate operation with no feedback from the wave model to the atmospheric model. In addition, the stand-alone runs are based on a later WAM cycle (Cy36r1). Since ERA-I (Cy31r2) there have been three updates to the IFS WAM code (see http://www.ecmwf.int/en/forecasts/documentation-and-support/changes-ecmwf-model). In Cy33r1 (June 2008) the shallow water physics were improved by modifying the nonlinear source term (Snl) and a new advection scheme was implemented, reducing the garden sprinkler effect (GSE). In Cy35r3 (September 2009) the wave damping was intensified by including a weak negative term in the wind input source term (Sin), mainly affecting the longer wave components–reducing swell. In Cy36r1 (January 2010) the wave model resolution was increased from 0.36° to 0.25° . However, for this particular experiment the resolution was set at 0.36°, going from ~110 to ~40 km. Further, the bathymetry was refined from ETOPO5 (http://www.ngdc.noaa.gov/mgg/global/etopo5.html) to ETOPO2 (http://www.ngdc.noaa.gov/mgg/fliers/01mgg04.html), which better represents areas of partial blocking. The number of spectral frequencies (30) and directions (24) are unchanged. The WAM-AS was run with slightly improved bias corrections of the altimeter data (i.e., ERA-I used to have a nonoptimal bias correction up until the end of January 2010). Figure 1 presents the mean discrepancy in H_s between ERA-I and WAM-AS over the period 1992–2011, which illustrates the main features mentioned

above. ERA-I is in general higher in the tropics because of less swell damping and higher in the lee of poorly resolved islands and shoals. The GSE is particularly evident east-northeast of Hawaii.

c. Observations: In situ and Envisat

In an attempt to validate trends we use a selection of 23 in situ observations, H_s and U_{10}. We emphasize the H_s data as they are not assimilated, but we also include U_{10} for comparison. The hourly data are averaged over ± 2 h and centered around synoptic times (Bidlot et al. 2002). Only collocated data with ERA-I are used to calculate monthly means.

For the period November 2002–October 2010, a total of nine years, we have binned Envisat altimeter winds into $2° \times 2°$ latitude–longitude bins and collocated the "super observations" with U_{10}^{ANA} in time and space. The super observations represent altimeter data averaged along track corresponding to the model resolution. Like in situ H_s, altimeter U_{10} are not assimilated and therefore independent of ERA-I.

3. Method

a. Trend

As the probability density function (PDF) of H_s and U_{10} do not conform to a Gaussian shape, trend estimates should not be based on a simple regression. In the following, the magnitude of the trend is determined by (Sen 1968; Yue et al. 2002)

$$\text{Trend} = \text{median}\left(\frac{x_j - x_l}{j - l}\right) \quad \forall \quad l < j, \qquad (1)$$

where x represents the data at time j and l. This offers a robust estimate of any monotonic trend.

In the following, we apply the seasonal Kendall test, a nonparametric test of randomness (H_0) against trend (H_1), an extension of the Mann–Kendall test (Mann 1945; Kendall 1948) especially adapted to seasonal data with serial dependence (Dietz and Killeen 1981; Hirsch and Slack 1984). Let $X_i = (x_{i1}, x_{i2}, \ldots, x_{in_i})$ represent the monthly data of U_{10} and H_s, where n_i is the total number of entries from month $i = 1, 2, \ldots, 12$ (only one entry per year), then the seasonal Kendall statistics for month i is expressed by

$$S_i = \sum_{k=1}^{n_i - 1} \sum_{j=k+1}^{n_i} \text{sgn}(x_{ij} - x_{ik}). \qquad (2)$$

In case of missing data at time j or k, $\text{sgn}(x_{ij} - x_{ik})$ is set to zero. From Mann (1945), Kendall (1948), and Hirsch et al. (1982) we define $S' = \sum_{i=1}^{12} S_i$, having a mean and variance given by

$$E[S'] = \sum_{i=1}^{12} E[S_i] = 0 \quad \text{and} \qquad (3)$$

$$\text{var}[S'] = \sum_{i=1}^{12} \text{var}[S_i] + \sum_{i=1}^{12} \sum_{l=1}^{12} \text{cov}(S_i, S_l) \quad \text{for} \quad i \neq l, \qquad (4)$$

where $\text{var}[S_i] = n_{ig}(n_{ig} - 1)(2n_{ig} + 5)/18$ and n_{ig} represents the number of nonmissing data per month ($n_{ig} = n_i$ for complete series). According to Hirsch et al. (1982), cov $(S_i, S_l) = 0$ when S_i and S_l are independent random variables. However, this fails to hold for monthly lag-1 serial correlation as low as 0.2 (Hirsch and Slack 1984). In the following we use an estimate of the covariance term defined by Dietz and Killeen (1981), which is well documented in Hirsch and Slack (1984). A two-sided test for trend is based on the standard normal variate Z defined by

$$Z = \begin{cases} \dfrac{S' - 1}{(\text{var}[S'])^{1/2}}, & \text{if} \quad S' > 0 \\[2mm] 0, & \text{if} \quad S' = 0, \\[2mm] \dfrac{S' + 1}{(\text{var}[S'])^{1/2}}, & \text{if} \quad S' < 0 \end{cases} \qquad (5)$$

where H_0 is accepted when $|Z| < 1.96$, using a significance level of $\alpha = 0.05$.

As stated in Hirsch and Slack (1984) the covariance term defined by Dietz and Killeen (1981) should be used with some caution, such as for small sample sizes less than 10 yr and in situations where data are, in fact, independent (e.g., in cases of many missing data). In the following analysis we omit the covariance term when found appropriate. This will be stated in the text.

b. RHtestsV4—Homogenization

The RHtestsV4 is a software package developed to detect and adjust for sudden step changes, or shifts, inherent in time series for reasons other than climatic changes. Here, we use the tool to homogenize monthly in situ observations that have been altered because of, for example, hardware and software updates. Even though the RHtestsV4 is capable of detecting shifts by analyzing the observed time series (referred to as base series) solely by itself (Wang 2008a,b), Wang and Feng (2013) highly recommend the use of a homogeneous and well-correlated reference series for a more reliable result, especially when used in an automatic manner. In the following, we use collocated ERA-I data. Shifts are

detected based on the penalized maximal t (PMT) test (Wang et al. 2007; Wang 2008a), using the base-minus-reference series, which is assumed to have zero-trend and Gaussian errors.

Once any shifts have been established the different segments of the base series are adjusted according to the quantile-matching (QM) procedure presented in Wang et al. (2010, their section 5) and Vincent et al. (2012). In short, the empirical distributions of all detrended segments are matched. The software has shown promise in Gemmrich et al. (2011) and Vincent et al. (2012).

It should be noted that, even though possible, we have not run the RHtestsV4 with metadata describing buoy updates, which may have increased the performance of the RHtestsV4.

4. Results

We start off by investigating the mean difference in monthly-mean H_s and U_{10} between ANA–24-h forecast (ANA–FC24) and 24–48-h forecast (FC24–FC48) over the periods 1979–91 and 1992–2012, that is, before and after introducing wave height altimeter assimilation in ERA-I (see Fig. 2). The red color scale in Fig. 2 shows where H_s and U_{10} are decreasing with increased FCR, while the blue color scale shows the opposite. The discrepancies are mainly due to assimilation effects and reflect model bias. For instance, in Fig. 2b, H_s^{ANA} is relatively higher in the storm track of the northeastern Atlantic as the model has been corrected for a negative bias related to insufficient wave growth in the area. According to Hanley et al. (2010), the annual mean wave age is lower in the North Atlantic storm track as opposed to the North Pacific, related to a stronger mean intensity in the extratropical cyclones (Bengtsson et al. 2006) and a corresponding stronger wind climate (Sterl and Caires 2005). Further, waves are more fetch limited in the North Atlantic because of a more varied coastline, particularly near the southern tip of Greenland and in the lee of Iceland. Fetch will also vary with season resulting from ice extent. It is striking that the biggest difference between H_s^{ANA} and H_s^{FC24} seems to follow the mean ice edge of the winter season. In contrast, waves generated in the storm tracks of the Southern Hemisphere are far less fetch limited by land. And, since the mean wind direction is westerly, with a slight northerly component (see Hanley et al. 2010, their Fig. 4), ice extent is probably not affecting the mean wave growth in the same sense.

In the eastern tropical Pacific, an area more or less completely dominated by swell (Semedo et al. 2011), the assimilation effect is reversed. The model overestimates the presence of swell, so H_s^{ANA} is corrected down and

therefore relatively lower than H_s^{FC24}. In the following, our prime concern is how the model bias is dealt with over time. Comparing Figs. 2a and 2b, the latter period is clearly more influenced by assimilation. The corresponding plots made with U_{10}, Figs. 2c and 2d, do not show the same geographical differences between the two periods. However, there seems to be a more uniform strengthening of U_{10}^{ANA} in the latter period. For FC24–FC48 (Figs. 2e–h), the differences between the two periods are far less pronounced, indicating that the model is relaxing toward its own climate, neglecting bias corrections made at ANA.

To further illustrate the effect of assimilation, we plot the discrepancies in monthly-mean H_s and U_{10} integrated over the Southern Hemisphere (SH; >20°S), the tropics (20°S–20°N), and the Northern Hemisphere (NH; >20°N) between ANA–FC24 and FC24–FC48, see Figs. 3a–c and 3g–i. All ice-covered areas have been removed from the H_s and U_{10} data. During the 1980s the discrepancy between ANA–FC24 (in red) is fairly stable for both parameters, with an exception found in the NH where U_{10}^{ANA} is steadily increasing relative to U_{10}^{FC24}. In August 1991 there is an abrupt jump in H_s^{ANA} in all regions caused by the sudden introduction of altimeter observations. The effect is most pronounced north of 20°N, but clearly visible south of 20°S. In the tropics the effect is negative and slightly less distinct. After August 1991 there is a steady relative increase in H_s^{ANA} outside the tropics up until approximately 2006. This seems related to a similar behavior in U_{10}^{ANA} globally. Given the fact that wave conditions in the tropics are highly influenced by waves (swell) generated in the SH and NH, it is somewhat surprising to find a relative decrease in H_s^{ANA} in the tropics, especially since the "local" U_{10}^{ANA} also is increasing. In the last part of the period H_s^{ANA} and U_{10}^{ANA} are decreasing. Overall, the largest fluctuations in ANA–FC24 are found in U_{10} in the tropics, reflecting the poorer predictability in the area. Notice that the FC24–FC48 comparison (Figs. 3g–i in green) shows less fluctuation compared to ANA–FC24. This is as expected as the model is gradually becoming less influenced by assimilation with FCR. It should be added that U_{10}^{ANA} also shows evidence of minor step changes. In 2000, when QuikSCAT was first introduced, there is a clear drop in U_{10}^{ANA} south of 20°S (see Fig. 3g).

In Figs. 3d–f and 3j–l we present corresponding linear trends in H_s and U_{10} as obtained at different FCR. Again, trends are based on spatial averages over each region per month and only data from ice-free areas have been used. Globally, all trends are positive and significant (not shown). The strongest trends are obtained at ANA and decreasing with FCR. Trends in H_s are relatively stronger compared to U_{10}. South of 20°S trends
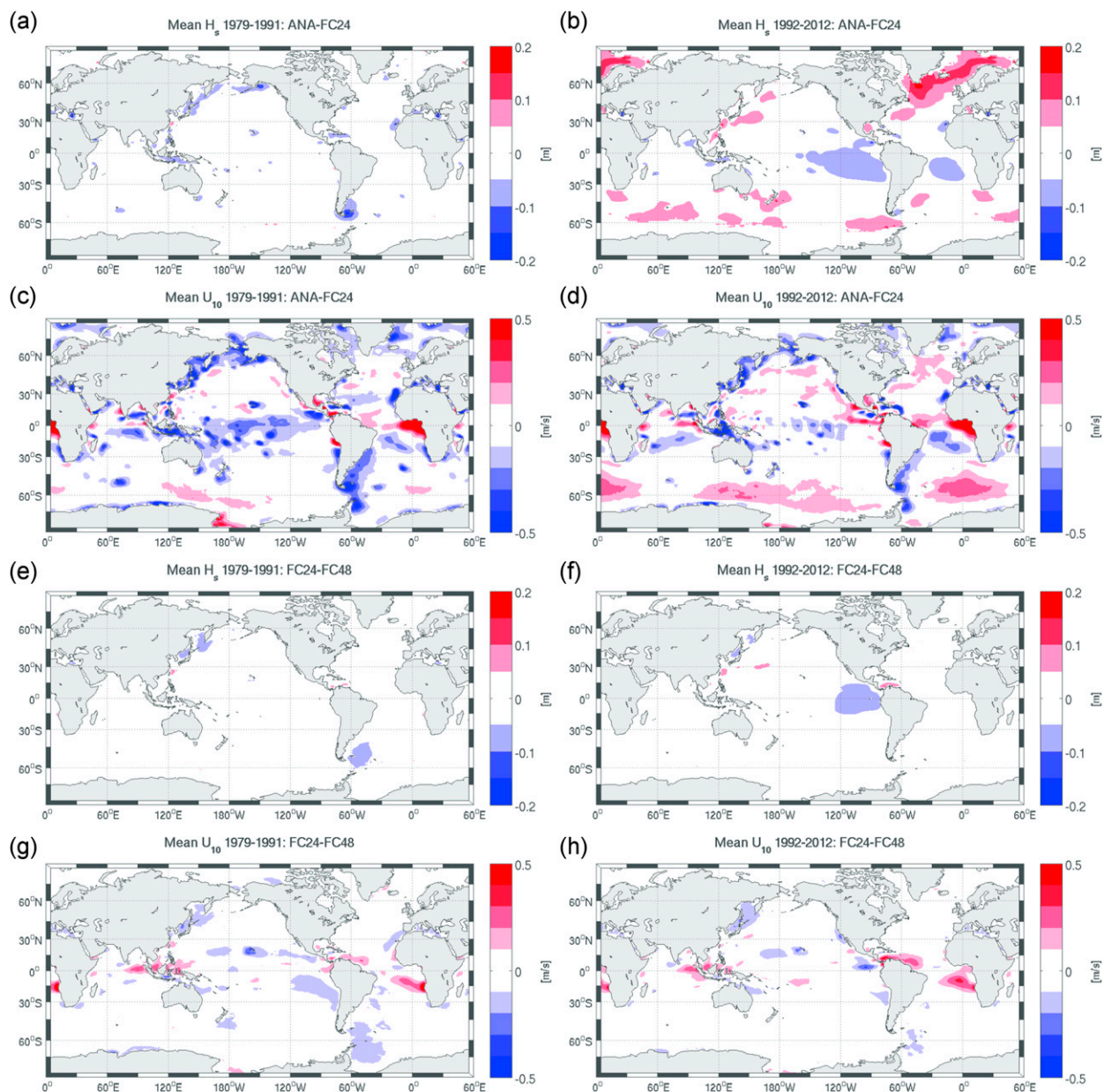
FIG. 2. Mean difference in H_s and U_{10} between (a)–(d) ANA–FC24 and (e)–(h) FC24–FC48 for the periods (left) before (1979–91) and (right) after (1992–2012) introducing wave altimeter assimilation in ERA-I.

behave much in the same manner. However, the trend in H_s is stronger and the trend in U_{10} is weaker compared to the global estimate. With the exception of U_{10}^{FC24}, U_{10}^{FC48} and U_{10}^{FC72} trends are significant. In the tropics all trends are positive and significant. This is the only area where the trend in H_s^{ANA} is weakest, or more correctly, most shifted toward a negative trend, which is clearly related to the effect of altimeter wave heights seen in Fig. 2b. North of 20°N only the trend in H_s^{ANA} is found to be statistically significant, contradicting the nonexisting trends found at increasing FCR.

In Fig. 4, we have made the same comparison as in Fig. 3 based on the mean area-integrated monthly-maximum H_s and U_{10}. For H_s, the biggest difference is found in the tropics where wave altimeter assimilation has an opposite effect, illustrated by the sudden relative increase in H_s^{ANA}. There is also a more prominent step change in H_s^{ANA} south of 20°S around the time *Envisat* and *Jason-1* became operational (i.e., the second half of 2003). Again, the discrepancy in FC24–FC48 (Fig. 4 in green) is more stationary compared to ANA–FC24. As with the monthly mean, U_{10}^{ANA} is generally increasing
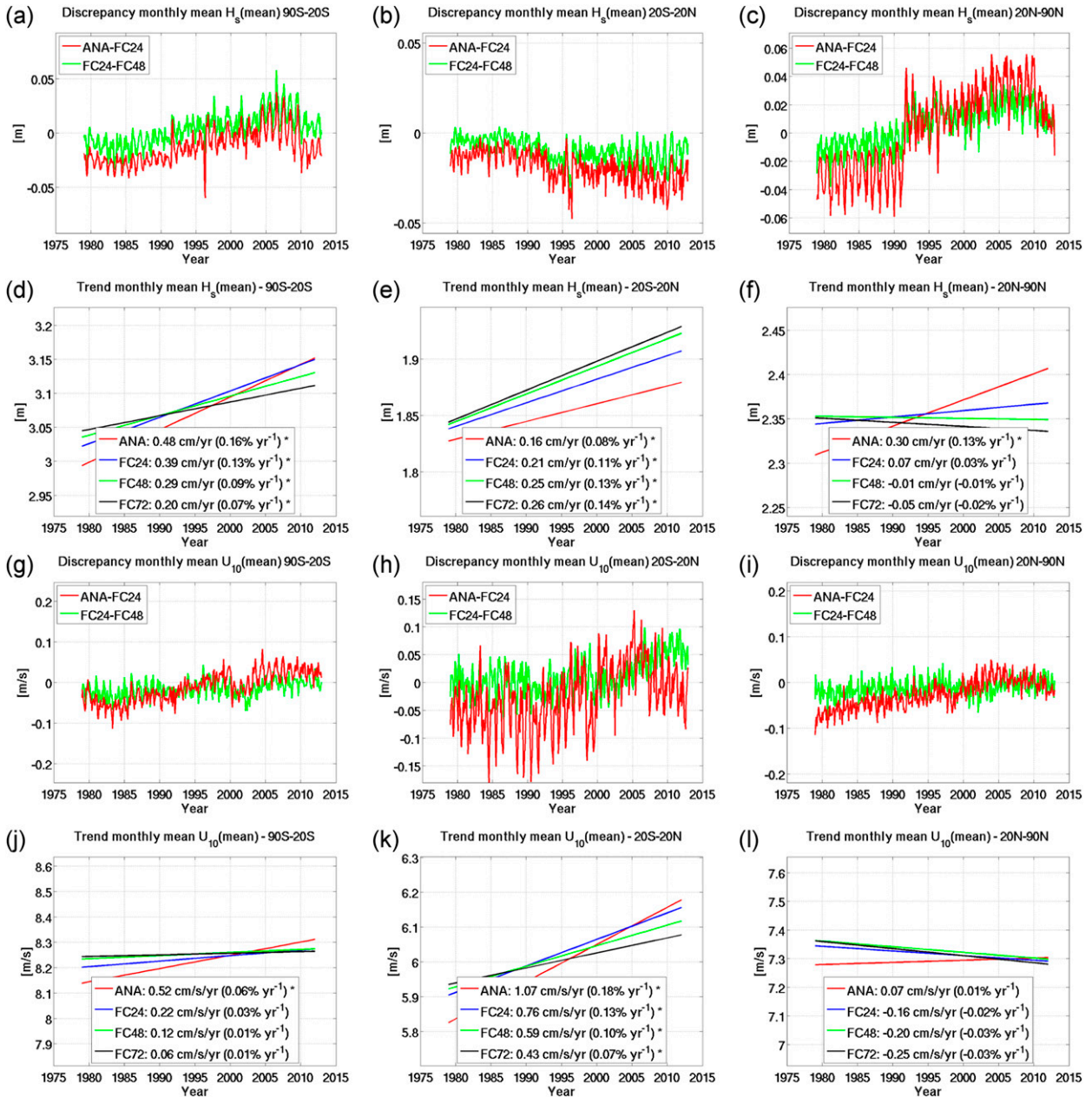
FIG. 3. (a)–(c) Discrepancy in monthly-mean H_s between ANA–FC24 and FC24–FC48, and (d)–(f) corresponding trend estimates from ANA, FC24, FC48, and FC72. Trends are presented in the legends and marked by an asterisk when statistically significant ($\alpha = 0.05$). The y axis have been scaled to span 6% and 10% of the mean H_s^{ANA}, respectively. (g)–(l) Corresponding results for U_{10}.

relative to U_{10}^{FC24} with time. In the tropics the discrepancies between ANA–FC24 and FC24–FC48 are both mainly positive, suggesting that the model needs more time in terms of FCR to relax to the model climate. Overall, the trends in mean monthly-maximum H_s and U_{10} are behaving quite similar to what seen in the monthly-mean data. Again, the effect of wave altimeter assimilation is found largest in H_s^{ANA} north of 20°N, causing a clearly contradicting trend compared to

corresponding estimates obtained at increased FCR. Globally (not shown), trends are positive and for the most part statistically significant, especially in H_s. This increase is primarily a result of the positive trends seen in the tropics and south of 20°S.

Figure 5 presents maps of trends in H_s^{ANA} and U_{10}^{ANA}, before and after wave altimeter data were first introduced, and over the full period. Between 1979 and 1991 there are primarily three areas showing significant
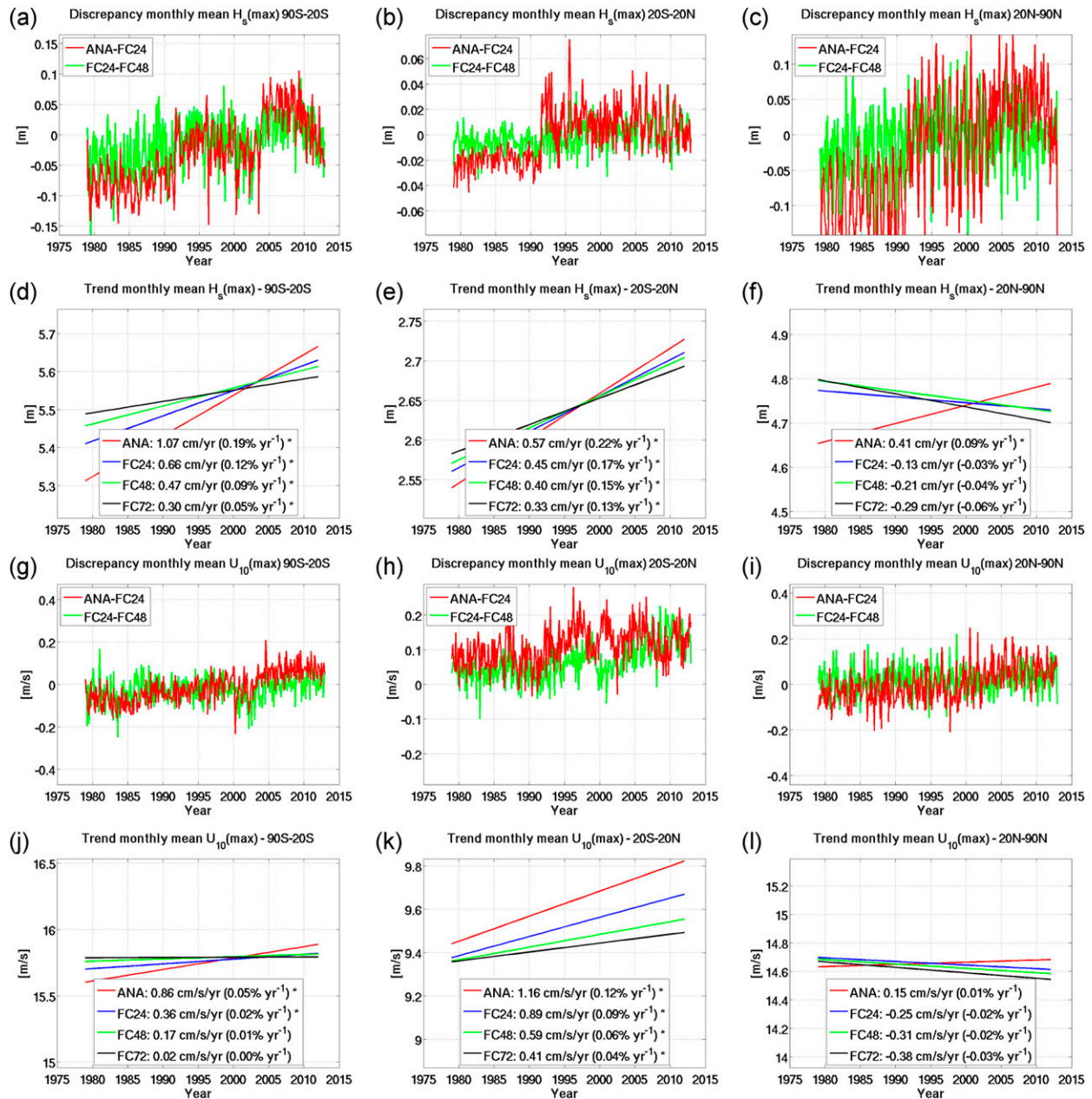
FIG. 4. As in Fig. 3, but for mean monthly-maximum H_s and U_{10}.

and positive trends in both H_s^{ANA} and U_{10}^{ANA}, near the Drake Passage off the southern tip of South America, in the South China Sea and in the northeastern Atlantic. Otherwise, significant trends are rare and scattered more randomly. For the latter period, the picture is more organized with a clear decrease in H_s^{ANA} in the northern central Pacific, weakly increasing in the central and southern Pacific (nonsignificant), increasing in the Gulf of Mexico and off the east coast of the United States. The most striking trend is found in U_{10}^{ANA} in the

central Pacific, an area highly correlated with El Niño–Southern Oscillation (ENSO). Since this area is dominated by relatively weak trade winds, the same signal is not equally apparent in H_s^{ANA}. When putting the two periods together, the strong increasing U_{10}^{ANA} trend in the central Pacific is damped because of a weaker or negative trend in the first period. However, H_s^{ANA} shows a larger area of positive significant trends than obtained by any of the two standalone periods. Even though the last period is almost twice the length of the first period
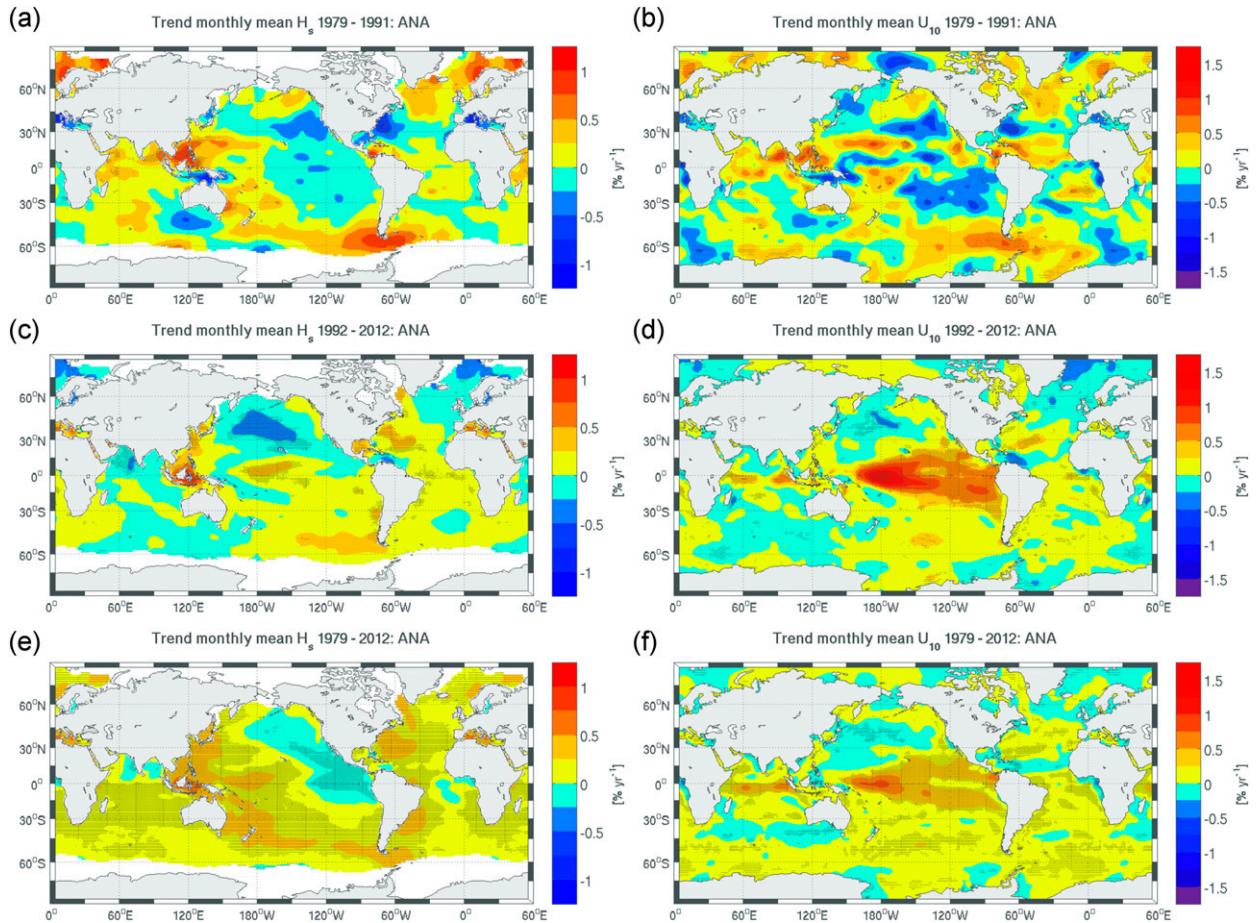
FIG. 5. (left) Trends in H_s^{ANA} presented in percentage relative to the mean H_s^{ANA} over the periods (a) 1979–91, (c) 1992–2012, and (e) and 1979–2012. (right) As in (left), but for U_{10}^{ANA}.

and therefore heavier weighted, the trends over the full period seem unrealistic, and must be seen in connection with the change imposed by the wave altimeter assimilation. For instance, we mentioned the northeastern Atlantic, where a larger area of positive and significant trends is obtained over the full period, as opposed to the two subperiods. This is directly related to the findings made in Figs. 2b and 3c but is not revealed by studying Fig. 5e alone.

In Figs. 6a and 6b we do the same comparison based on FC48. Trends are somewhat weaker and significant over a smaller area. The positive trends found in H_s^{ANA} in the northeastern Atlantic are now negative and nonsignificant. Similarly, the significant negative trends found in H_s^{ANA} in the eastern equatorial Pacific are shifted toward a positive trend, but still slightly negative north of the equator. The monthly maxima (see Figs. 6c,d) show similarities with the results obtained with the mean conditions, but are geographically more confined.

a. ERA-I versus in situ observations

In an attempt to validate the trends obtained with ERA-I at different FCR, we have used a selection of in situ buoy data situated along the Eastern Seaboard and the west coast of the United States and in the northeastern Atlantic. The time span and coverage are variable between locations. Trends are therefore not intercomparable. Only available data overlapping ERA-I have been used. Months with less than 50% coverage are censored. This threshold is somewhat arbitrary and will probably influence trends over the actual periods. However, here we do not focus on the trends per se, only the difference between modeled and observed trends, making this choice acceptable. All modeled data are consecutively interpolated to the positions of the buoys. Because some of the buoys have been subject to movement over time, only collocated data lying within $\pm 0.25°$ latitude/longitude of the median position have been used. In this way only data originating from the same climate are retained. Since most

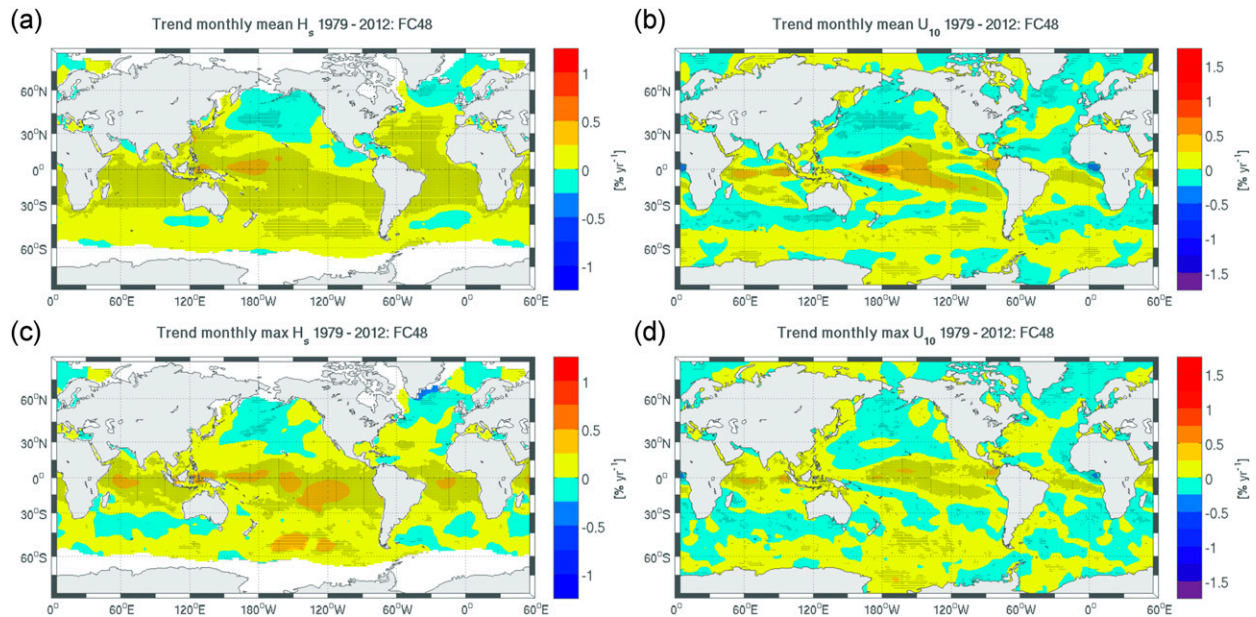FIG. 6. Trends in (a) monthly-mean and (c) monthly-maximum H_s^{FC48} presented in percentage relative to the corresponding mean value over the period 1979–2012. (b),(d) As in (a),(c), but for U_{10}^{FC48}.

of the buoys are regularly removed, serviced, recalibrated, and returned to service, step changes exist in the original time series (Gemmrich et al. 2011; Wan et al. 2010). We have applied the RHtestsV4 (presented above), a homogeneity tool, in an effort to compensate for these changes. We use H_s^{FC24} as a reference series. An example of the software output is presented in Fig. 7, illustrated with H_s data from the position of buoy 46036. At the top, the original observations (BASE) and collocated H_s^{FC24} data (REF) are plotted together with corresponding trends. In the middle, the base-minus-reference series is plotted in blue, which constitute the basic data for detecting nonclimatic steps. Detected mean shifts are presented by the black line, while the QM fit is shown in red. Notice that the QM fit has seasonal variations, ultimately correcting the BASE series differently according to season. In the bottom plot, the original observations are shown together with the corrected observations according to the QM fit, with corresponding trends.

The result of the trend comparison is illustrated in Fig. 8. The top plot presents the data coverage per station and the trends obtained with the original observations, the corrected observations and ERA-I. Eight out of 23 locations do not contain data overlapping for August 1991. Results are therefore unaffected by the step change imposed by the altimeter data in ERA-I. Notice that there are a number of locations where the observed trend based on the original data clearly deviates from ERA-I. Be aware that these deviations are

perceived as large because the trends themselves are weak. However, "outliers" are effectively adjusted with the RHtestsV4. In the middle row we have color coded the FCR producing the minimum and maximum absolute error in trend relative to the original observations. Seven out of 23 observed trends are statistically significant. From these, H_s^{ANA} validates best at only one location (44008). In fact, in 14 out of the 23 (~60%) cases H_s^{ANA} offers the poorest representation of the trend relative to the original observations. In 10 out of 23 cases the best estimate of the trend is obtained with H_s^{FC48}. When performing the same comparison based on the corrected observations, shown in the bottom of Fig. 8, the result is similar: H_s^{ANA} performs worst at 12 out of 23 locations, more than 50%. In seven cases H_s^{FC48} performs best, while H_s^{FC24} performs best at nine locations.

Despite the fact that in situ U_{10} buoy observations indeed are assimilated in ERA-I we have conducted the same analysis with U_{10} (see Fig. 9) as this may support some of the results obtained with H_s. Expectedly, U_{10}^{ANA} is performing better then H_s^{ANA} relative to the corresponding original observed trends, showing the least discrepancy at 12 out of 23 locations. However, with the adjusted observations, the result is different. Now, only one location offers a significant trend, compared to 13 from the original observations; U_{10}^{ANA} is performing worst at 14 locations, while U_{10}^{FC24} and U_{10}^{FC48} combined perform best at 18 locations.

The choice of using the FC24 as a reference series in the RHtestsV4 is based on the fact that it correlates well
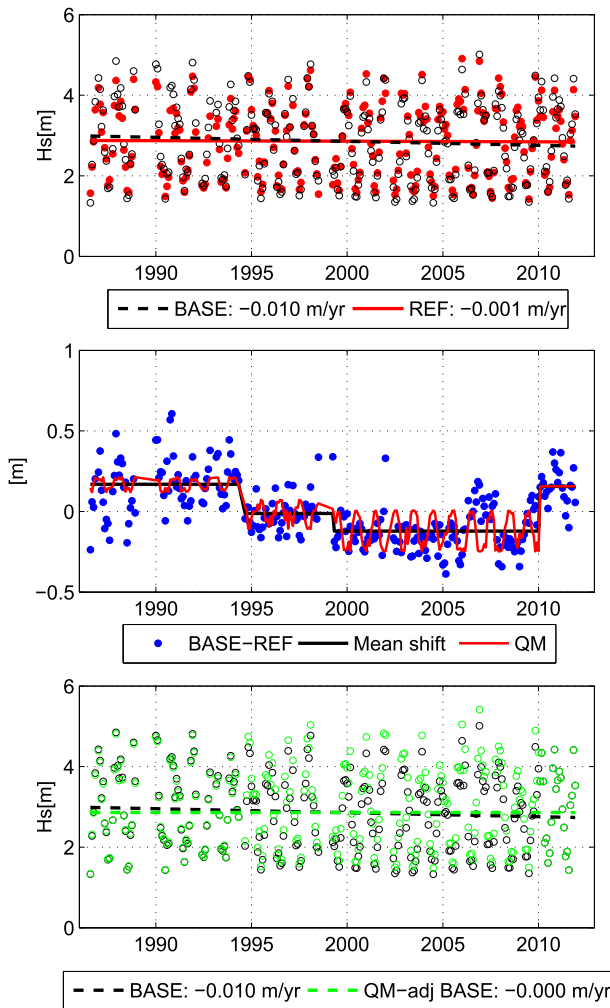
FIG. 7. Adjusted trend estimates of H_s from buoy 46036 based on the homogenization software RHtestsV4. (top) Collocated monthly-mean H_s from in situ (BASE) in black and ERA-I at FC24 (REF) in red with corresponding trends. (middle) Discrepancy between BASE and REF, accompanied by the detected mean shifts and the QM fit. The QM-adjusted BASE series uses the last segment as a reference level. In this particular case, the BASE series is adjusted slightly down until about 1994 and lifted over the period 1994–2010. (bottom) The BASE series together with the QM-adjusted BASE series. Original and adjusted trends are presented in the legends.

with observation without being directly affected by assimilation, unlike ANA. However, we do acknowledge the fact that trends obtained with the adjusted observations tend to approach the trends inherent in the reference series. This is confirmed when producing similar maps to those presented in Figs. 8 and 9 using ANA and FC48 as reference series. This will affect the analysis. Because of the number of missing data, all significant trends presented in Figs. 8 and 9 are based on Eq. (4) setting the covariance term to zero. When running the

same test with the covariance estimate proposed by Dietz and Killeen (1981), none of the trends is found to be statistically significant, either for U_{10} or H_s.

b. EC-WAM run with and without altimeter wave height assimilation, 1992–2011

Because the wave height altimeter assimilation in ERA-I comprises measurements from a number of satellite missions, transitions between missions may create spurious trends if calibration is inadequate. By investigating the discrepancy in monthly-mean H_s between the two stand-alone WAM runs any step changes due to wave altimeter assimilation may be detected. Ideally, the discrepancy between the two runs should be stationary. As described above, the WAM cycle used in the two stand-alone runs (cycle Cy36r1) is not identical to the WAM cycle used in ERA-I (cycle Cy31r2) and they are therefore not strictly comparable. However, any changes in trends between the stand-alone runs, should shed light on issues also inherent in ERA-I. In Fig. 10 (left) we have plotted the monthly discrepancy in mean global H_s as obtained with the two runs. The different satellite periods are color coded: *ERS-1* (pink), *ERS-2* (purple), *Envisat* (green), *Jason-1* (yellow), and *Jason-2* (cyan). Most apparent, there is a substantial bias between the two runs. The altimeter assimilation is adding approximately 20 cm to the mean global H_s (~8%). Because of the substantial model bias, periods with reduced altimeter assimilations are fairly easy to identify, as they represent periods of more coherent model results, here illustrated by local minima (spikes). Over the 20-yr period there are four months where the discrepancy between the two runs goes below 0.1 m: April 1992, March 1999, February 2001, and July 2003. In fact, in February 2001 no altimeter data are assimilated and the two model runs are essentially the same, illustrated by the nonexisting discrepancy. This clearly indicates how H_s is affected by the changing number of altimeter assimilations. Similarly, between May 1995 and June 1996 both *ERS-1* and *ERS-2* were in orbit, offering more altimeter data, more effectively correcting model bias and increasing the discrepancy between the two runs. Somewhat surprisingly, from the time *Jason-2* was operating (i.e., February 2010), there were three satellites providing altimeter H_s; still, the discrepancy between the two runs was reduced, having an opposite effect to that indicated above. Also notice that there is a clear reduction in the standard deviation between the two datasets from this point on. Overall, the discrepancy between the two stand-alone WAM runs seems to be affected by the transition from one satellite to the next, but with variable effect. This is confirmed by the same plot made with the mean global max H_s (not
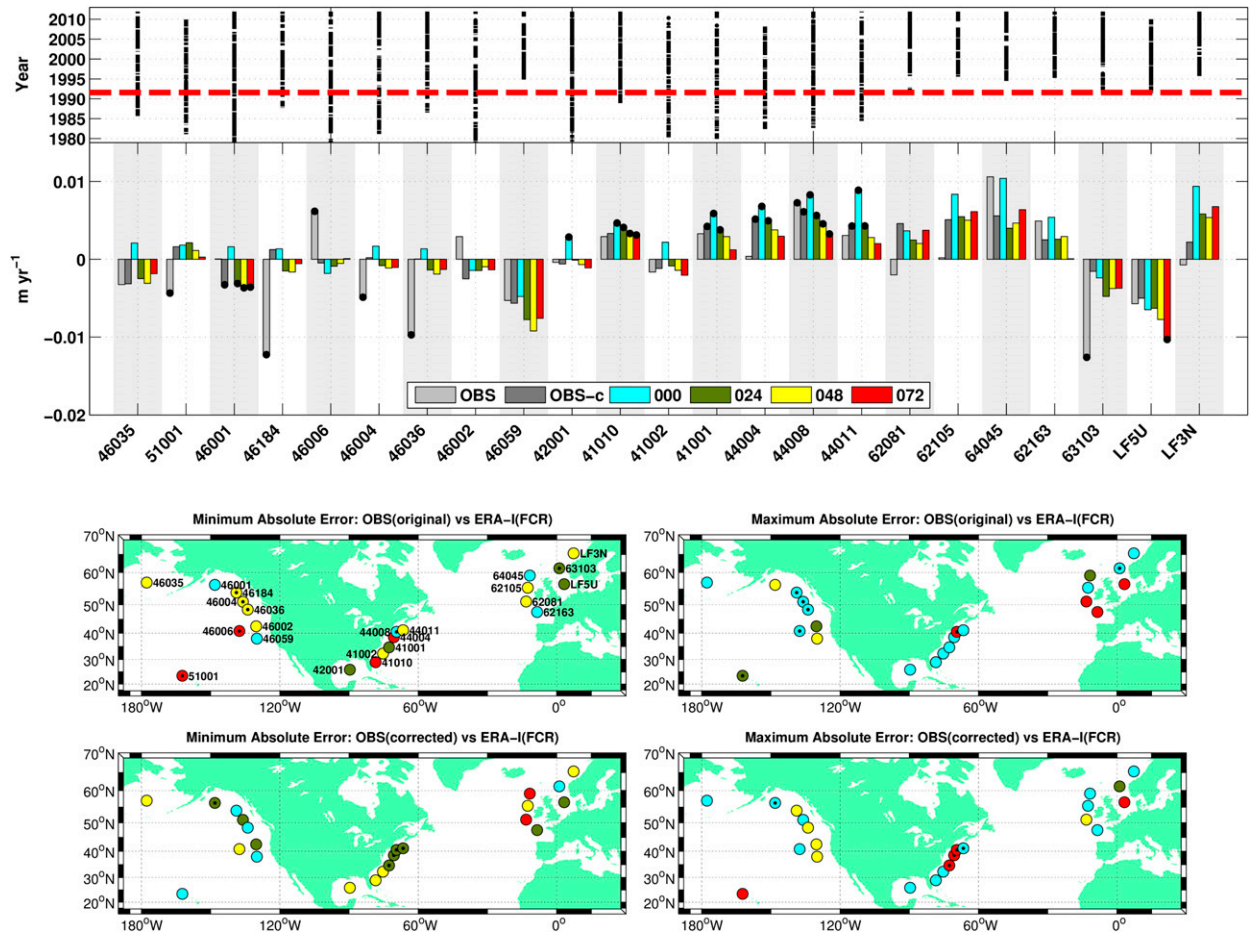
FIG. 8. Comparison of trend estimates from monthly-mean H_s from collocated observations and ERA-I at 23 locations. (top) Data coverage per location (red line indicates when wave altimeter data was first introduced in ERA-I) and trend estimates based on the original observations (light gray), corrected observations (dark gray) and for ERA-I at ANA (cyan), FC24 (dark green), FC48 (yellow), and FC72 (red). Significant observed trends are marked by a black dot and are based on Eq. (4) omitting the covariance term. (middle) The FCR (color coded as at top) showing the (left) minimum and (right) maximum absolute error in trend compared to observations. Black dots mark where the observed trend is statistically significant. (bottom) The FCR (color coded as at top) showing the minimum and maximum absolute error in trend compared to adjusted observation. Black dots mark where the observed (adjusted) trend is statistically significant.

shown), which shows the same features. More importantly, the total number of altimeter assimilations needs to be steady, and may potentially affect the data homogeneity far more. Based on the mean global H_s there is no clear trend in the discrepancy between WAM-AS and WAM-NAS; however, when inspecting the corresponding spatial trend, there are clear differences, see Fig. 10 (right). Cyan and blue indicate areas where WAM-AS is decreasing relative to WAM-NAS (i.e., areas where assimilation has a negative contribution on trends). This is most prominent in the eastern central Pacific, especially near the Galápagos Islands, and south-southeast of South Africa. In the North Atlantic the impact of altimeter assimilation is significant and positive.

In Fig. 11 we present the trend in H_s as obtained from the two stand-alone WAM runs together with H_s^{ANA} and H_s^{FC240}, spanning the same period. The main features of the stand-alone runs (a) and (b) are similar. Going into detail, the WAM-NAS shows a stronger positive trend in the eastern Pacific, particularly in the tropical and southern part, and a slightly more negative trend in the northeastern Atlantic. These differences are directly connected to the findings made in Fig. 10 (right). When comparing the trend in H_s of the stand-alone runs with the trend in U_{10} in Fig. 5d, which is spanning approximately the same period (i.e., 1992–2012), it is worth noting that WAM-NAS comes closer in resembling the U_{10} trend. Because of the significant discrepancy between the two stand-alone runs, see Fig. 10 (left), it is
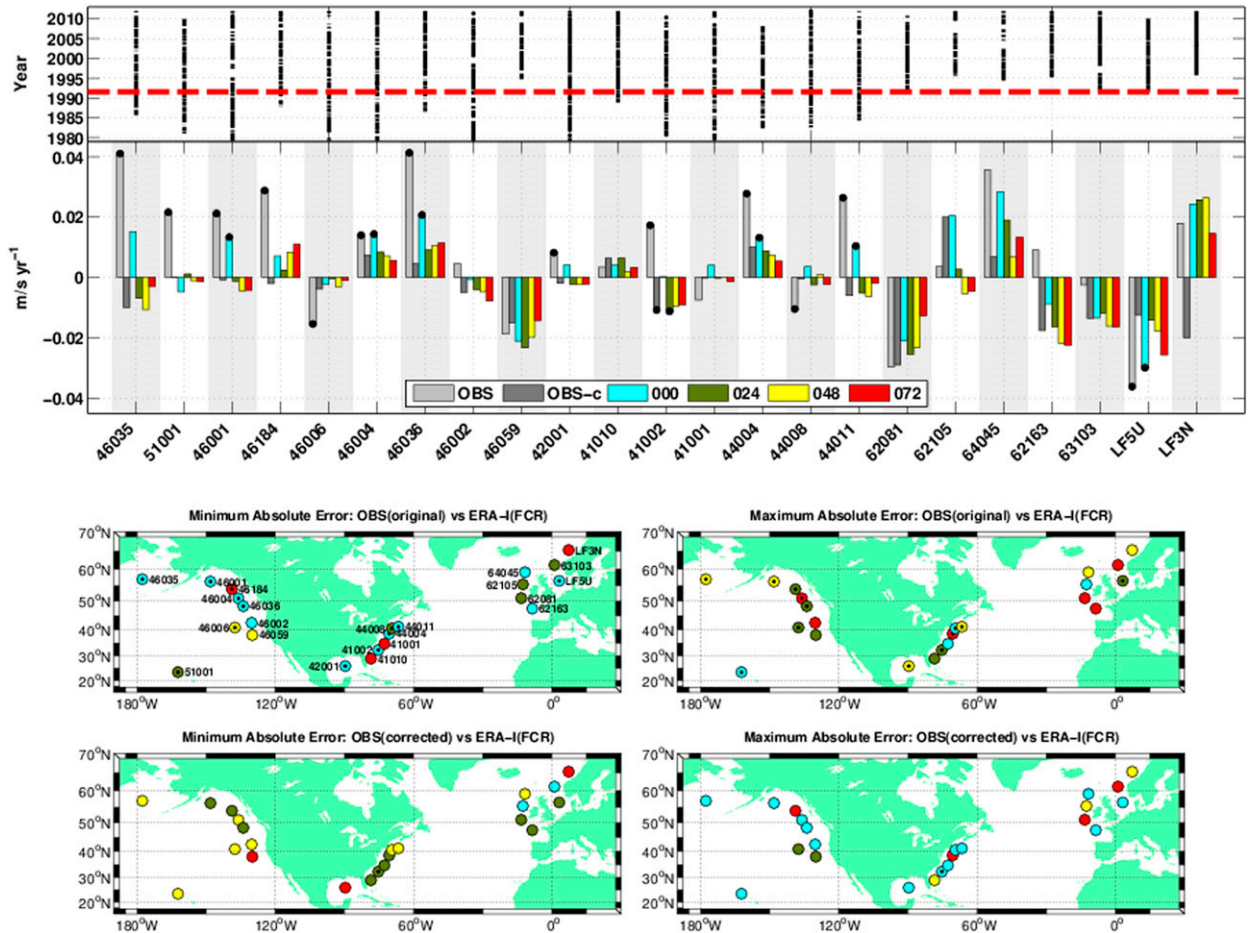
FIG. 9. As in Fig. 8, but for U_{10}.

plausible that WAM-AS is closer to saturation initially, while WAM-NAS, which is biased low (~0.2 m), is behaving more like the U_{10} trend, with more room for wave growth as U_{10} increases over time. However, there is no arguing the fact that certain transition periods introduce nonclimatic steps, which probably is the main reason why WAM-AS and WAM-NAS show different trends in certain areas.

The comparison between WAM-AS and H_s^{ANA} [i.e., Figs. 11a,c] shows a closer resemblance, as would be
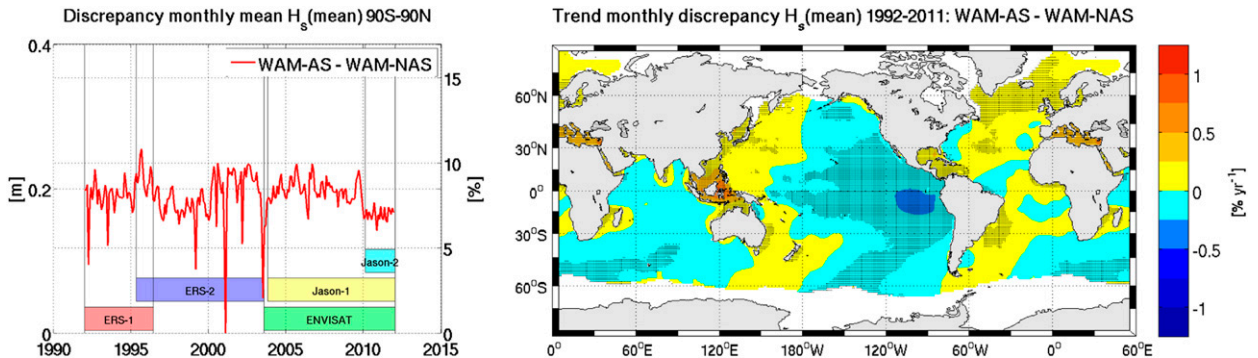

FIG. 10. (left) Monthly discrepancy in mean global H_s between the two stand-alone EC-WAM runs with and without wave altimeter assimilation. Satellite missions are color coded: *ERS-1* (pink), *ERS-2* (purple), *Envisat* (green), *Jason-1* (yellow), and *Jason-2* (cyan). (right) Trend in monthly discrepancies between WAM-AS and WAM-NAS presented in percentage relative to WAM-AS.
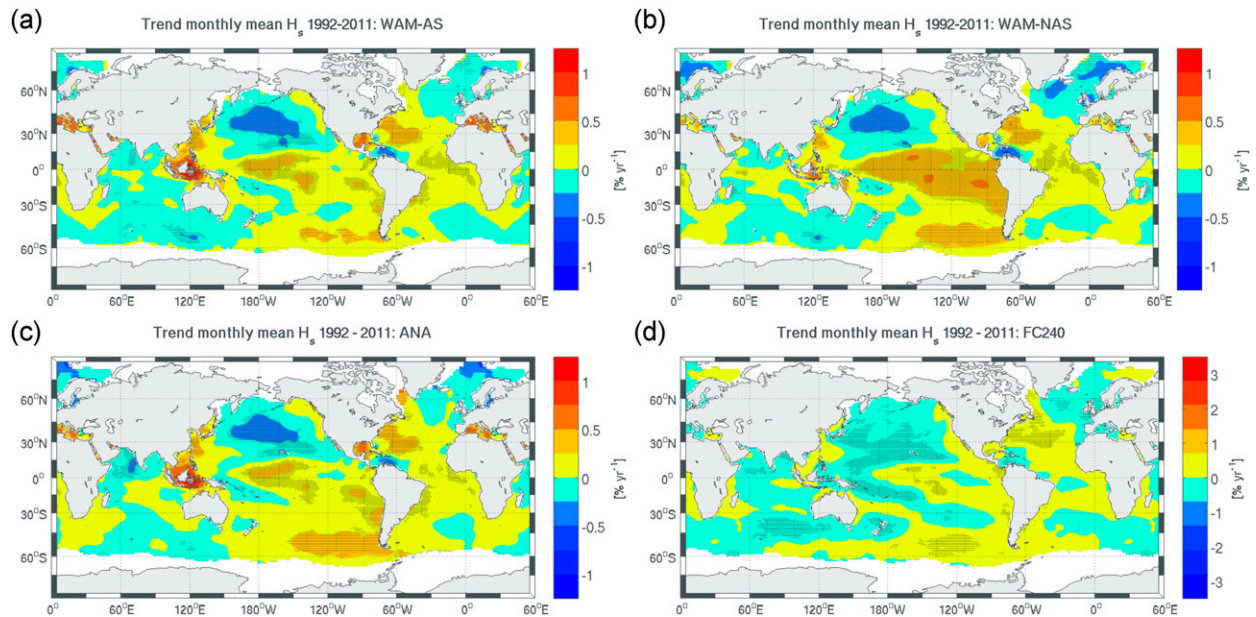
FIG. 11. (top) Trends in H_s obtained with two stand-alone WAM runs (a) with and (b) without wave altimeter assimilation over the period 1992–2011 presented in percentage relative to the respective mean H_s. (bottom) Corresponding estimates for (c) H_s^{ANA} and (d) H_s^{FC240}.

expected. Even though the wind forcing is not strictly identical, any nuances are equally likely a result of different model physics, as this may affect the wave field differently depending on wave conditions. Nevertheless, changes in wave altimeter assimilation are probably the biggest contributor. By investigating the trend in discrepancy between H_s^{ANA} and WAM-AS (not shown), we find that H_s^{ANA} is increasing in the majority of the SH. In areas where the trend is significant, H_s^{ANA} increases by approximately 0.05–0.1 yr^{-1} relative to WAM-AS. Still, this is not enough to impose drastically different trends in H_s.

In Fig. 11d, we present the trend in H_s^{FC240}. The 10-day (240 hr) ERA-I forecast (FC240) should be more or less unaffected by assimilation, and in that sense comparable with WAM-NAS; however, H_s^{FC240} is forced by 10-day prognostic wind fields and does not allow a direct comparison with the three other plots. Nevertheless, most of the features found at ANA are recognizable in H_s^{FC240}, but less pronounced.

c. Envisat altimeter winds: November 2002–October 2010

In a similar fashion, we want to validate trends in U_{10} from ERA-I against corresponding estimates based on data unaffected by assimilation. For the period November 2002–October 2010, a total of nine years, we have binned reprocessed *Envisat* altimeter winds into 2° × 2° latitude–longitude bins and collocated the super

observations with U_{10}^{ANA} in time and space. The super observations represent altimeter data averaged along track corresponding to the model resolution (Dragani et al. 2015). This represents a consistent dataset and uses the same wind speed algorithm as in Abdalla (2012). In Figs. 12a and 12b we present trends obtained from the two datasets. Notice that the color scale spans a wider range than applied for U_{10} in Fig. 5, from −3.5% to 3.5% yr^{-1} versus from −1.75% to 1.75% yr^{-1}, indicating that the shorter period inherent much stronger trends. The two plots compare remarkably well, with trends in excess of 3% yr^{-1} in the western equatorial Pacific, an increase of almost 30% in nine years. This area is highly correlated with the Southern Oscillation index (SOI), that is, the normalized pressure difference between Tahiti, French Polynesia, and Darwin, Australia (Boisséson et al. 2014; Stopa et al. 2013). Over the period in question the SOI was fluctuating, but mainly increasing, going from a situation with low pressure differences and weak trade winds (El Niño type) to a situation with increased pressure difference and stronger than normal trade winds (La Niña type). Further, we find a decrease in the northwest Pacific, but this area shows a more scattered significant result. In the South Pacific, toward Cape Horn, trends are positive, statistically significant and highly comparable.

The temporal coverage of *Envisat* is limited by the polar-orbiting period of approximately 100 min and repeat cycle of 35 days. The collocated ERA-I data will
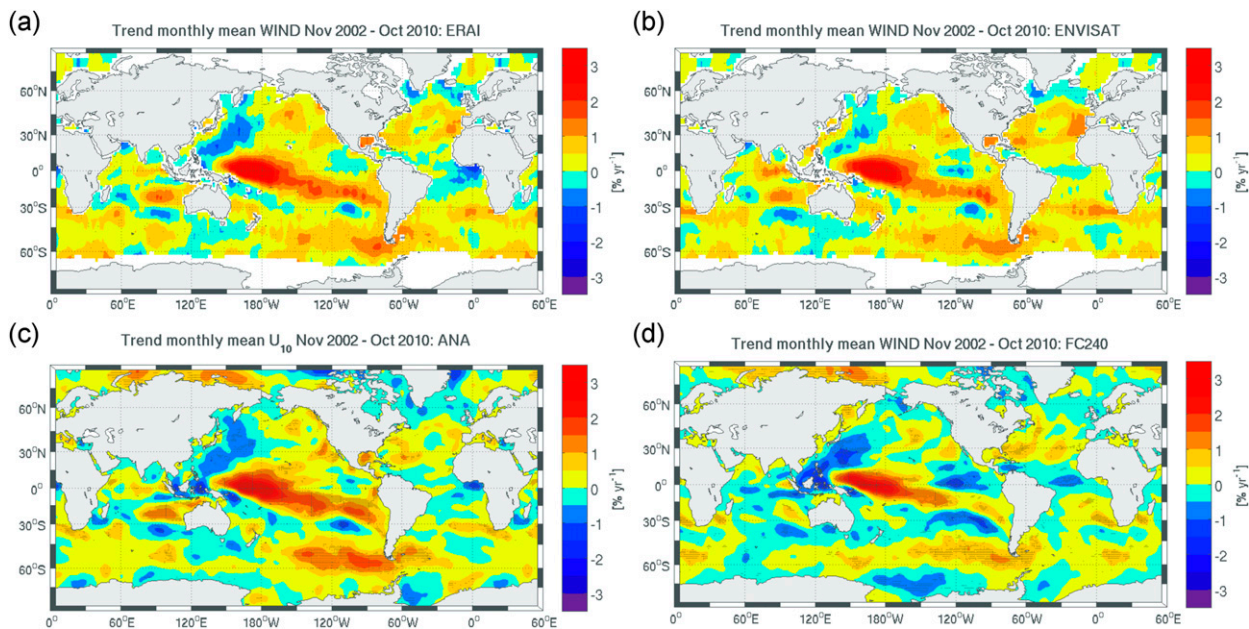
FIG. 12. (top) Trends in U_{10} obtained with collocated data from (a) U_{10}^{ANA} and (b) *Envisat* over the period November 2002–October 2010 presented in percentage relative to the respective mean U_{10}. (bottom) Similar estimates based on (c) U_{10}^{ANA} and (d) U_{10}^{FC240} using all available data over the same period. The significance test is based on Eq. (4) omitting the covariance term because of the limited period.

only constitute a fraction of the full dataset. To illustrate any loss of signal/trend due to subsampling, we present the trend in U_{10}^{ANA} based on all available data over the same period. Comparing trends obtained with ERA-I from the full and collocated dataset, the main features are retained (see Figs. 12a,c). Going into detail, the full dataset seem to be shifted slightly toward negative trends (blues and cyan). However, when comparing areas of significant trend, the result is quite comparable, which supports the use of coherent wave altimeter data for trend analysis.

As before, it is of interest to investigate how much trend is retained at FC240 (see Fig. 12d). Even though the main features are clearly intact, it seems the trend in general is shifted in a negative direction.

5. Discussion

In the preceding analysis we have investigated trends in H_s and marine U_{10} obtained with ERA-I at different FCR. The study was motivated by the following questions. First, does the sudden introduction of wave altimeter assimilation in August 1991 introduce a step change in the H_s statistics in ERA-I, and therefore impose spurious trends? Second, does the different satellite updates within the era of altimeter assimilation also affect H_s trends? Third, is the U_{10} statistics changing as a result of nonstationary assimilation? Fourth, if spurious trends are present at ANA, are better trend estimates

obtained at increased FCR? If so, which one performs best?

Wave altimeter assimilation will have the biggest impact in areas of increased model bias. Its effect is largely positive in forecasting, but for reanalysis, sudden corrections will affect trends. In this study, we detect the largest model bias in H_s in the northeastern Atlantic, an effect of too weak wave growth off Newfoundland, south of Cape Farewell, and south of Iceland, areas with intense cyclone activity (Bengtsson et al. 2006; Ulbrich et al. 2009; Hodges et al. 2011) and often fetch limited conditions. The bias extends northeast with the mean wave direction and seems to follow the winter ice extent to the north. The same area shows the largest discrepancy in H_s trend at ANA and increased FCR. Even though the trend in H_s^{ANA} is statistically significant, it is clearly spurious. The trend is also reinforced by steady increasing winds over the period (see Fig. 3i) but not to the extent that the trend in U_{10} is drastically different at ANA and increased FCR (see Fig. 3l). For the Southern Hemisphere (>20°S) the effect of altimeter wave height assimilation is similar, but less pronounced. No areas stand out like the northeastern Atlantic, even though the area in general is biased slightly low (see Fig. 2b). In the tropics the positive trend in the mean integrated H_s^{ANA} is counteracted by the altimeter wave height because of a positive bias in the wave model. Unlike the NH/SH, the trend in H_s^{ANA} is weaker than corresponding estimates obtained at increased FCR. This is mainly

seen in the eastern tropical Pacific and central Atlantic, areas dominated by swell, which is overestimated by ERA-I. Trends in the integrated mean monthly-maximum H_s and U_{10} are comparable with those based on monthly-mean conditions. The biggest difference is found in the tropics, where the wave model clearly possess a negative bias for the highest wave conditions, which is corrected for after August 1991 (see Fig. 4b). Again, the most striking result is found in the northeastern Atlantic where H_s^{ANA} is indicating a clear increase in the extreme events, while all the corresponding estimates at increased FCR are negative (see Fig. 4f).

The H_s and U_{10} trend estimates obtained with ERA-I are validated against the corresponding estimates from in situ data. The comparison is challenging in several ways: most time series are fairly short; they span different periods and have missing data; they contain intrinsic nonclimatic step changes and the buoys are located in areas of rather weak trends, often nonsignificant. In addition, the U_{10} data have been assimilated into ERA-I and are therefore not independent. Even though most of these issues are undesirable, they do not contaminate the data. Step changes imposed by buoy updates, on the other hand, are a direct source of error that needs to be addressed and accounted for when estimating trends. This being said, an accurate homogenization of in situ data is a complicated task and a study in itself. Here, we use the RHtestsV4 package, a homogenization tool that has showed promise in similar studies in the recent past (Gemmrich et al. 2011; Wan et al. 2010; Vincent et al. 2012). To optimize the performance of the tool, it is encouraged that the user incorporate dates of expected nonclimatic steps (metadata). As this is often difficult to acquire, and in this study too comprehensive, the tool may be run with a highly correlated reference series, providing a base-minus-reference series used to detect steps. This has one important implication. Any step changes inherent in the reference series will falsely detect steps in the base series. In other words, H_s^{ANA} does not make a good reference candidate. So, in the following we use FC24 for wind and waves as a reference, as these data are well correlated with the in situ measurements and less affected by assimilation. To test the robustness of the result, we have applied the same homogenization routine using FC48 and FC72 as the reference. By studying similar plots to Fig. 7, we find that the results are sometimes comparable, but occasionally very different from those obtained with FC24 as reference. This has mainly two explanations: the correlation between the base and reference series deteriorates with FCR and creates a noisier base-minus-reference series, making it harder to detect steps; more importantly, most trends

are very weak and often nonsignificant. Only small changes are required to change the resulting trends. In fact, comparing trends that are statistically nonsignificant is in itself not prudent. These factors reduce the confidence in the trend estimates obtained with the adjusted in situ data, and the comparison. When we still choose to perform the analysis, it is because in situ observations constitute very important data in wave model validation and are therefore a logical place to start.

Trends obtained with the uncorrected H_s observations are comparable with Gemmrich et al. (2011) (Fig. 1b), but are generally weaker, which probably is an effect of the different time periods used and different data processing (e.g., using monthly versus daily mean data). As in Gemmrich et al. (2011), we find that our H_s trends are weakened when homogenized with the RHtestsV4. The main findings of Fig. 8 are as follows: out of 23 locations, the H_s^{ANA} trends show maximum absolute error at more than 50% of the locations, both when compared to the original observations and the adjusted observations. Note that H_s^{FC48} performs best in approximately 45% of the cases relative to the uncorrected observations, while H_s^{FC24} and H_s^{FC48} combined show least absolute error at approximately 70% of the locations when compared to the adjusted observations. The U_{10}^{ANA} trends perform best relative to the uncorrected observations in more the 50% of the cases. This is expected because the datasets are dependent through assimilation. When compared to the corrected observations, U_{10}^{FC24} and U_{10}^{FC48} combined outperform the rest at approximately 80% of the locations, while U_{10}^{ANA} performs worst in more than 60% of the cases. There are no definite conclusions to be drawn from these results, for this the dataset is too small and uncertain. However, one might summarize as follows: trends in H_s^{FC24} and H_s^{FC48} validate better than H_s^{ANA}. Similar results are obtained with U_{10} when compared to observations corrected for nonclimatic step changes. The U_{10}^{ANA} trends compares best with the original observations simply because they are dependent through assimilation.

We have investigated the impact of satellite updates on H_s trends by analyzing two stand-alone runs, with and without wave altimeter assimilation. As these runs differ from ERA-I in several ways, we are not setting out to explain the minor differences seen in H_s trends between ERA-I and the corresponding WAM-AS. We simply acknowledge that the two runs produce very similar trends, and therefore conclude that any issues detected by comparing the two stand-alone runs probably also apply to ERA-I H_s, or at least have similar implications. From the preceding analysis we find that discontinuities in H_s (in means and maxima) often are related to altimeter updates or altimeter availability. Since the wave

model is biased low (~ 0.2 m), the lack of altimeter data may potentially influence the data homogeneity quite severely, further affecting trends. This is for instance emphatically demonstrated by ERA-I where altimeter data are suddenly introduced in August 1991.

We find no single event affecting the U_{10}^{ANA} trends the same way as experienced with H_s^{ANA} in the northeastern Atlantic. Nevertheless, there are strong indications that step changes of variable magnitude, also exist in the U_{10} data, but they are generally smaller. One example is seen in the beginning of 2000 when QuikSCAT was first introduced in ERA-I, which clearly had an impact in the SH. Because of the sparsely distributed conventional wind observation in the SH, the model is more influenced by satellite data here. When comparing trends in U_{10} from *Envisat* with collocated ERA-I data over the period November 2002–October 2010, the correspondence is impressive. This underpins that U_{10}^{ANA} are less affected by nonstationary assimilation, at least over this period.

In this study, in the context of trends, we portray nonstationary assimilation as a source of error. But is it all bad? Trends in H_s and U_{10} obtained with ERA-I will be affected by assimilation on all FCR, but with a diminishing effect. Going to FC240 (i.e., the 10-day forecast), assimilation should have an insignificant effect on trends. In Figs. 11d and 12d, we have plotted trends obtained with FC240 for H_s and U_{10}, respectively. From this, it is our general impression that FC240 offers weaker trends compared to ANA, or shifted slightly toward the negative. This result is supported by the findings made in Figs. 3 and 4, where U_{10}^{ANA} shows a more positive trend compared to trends at increased FCR. Even though trends obtained at FC240 clearly preserves the spatial features found at ANA well, there seems to be a trade-off between removing the positive impact of data assimilation at longer FCR and getting lower level of uncertainty in the predictions at shorter FCR.

In Stopa and Cheung (2014, their Fig. 15) the trend in monthly discrepancy between H_s^{ANA} and altimeter wave height from *Geosat*, TOPEX/Poseidon, and *Geosat Follow-On* (*GFO*) is presented, which reflects the error trend in H_s^{ANA}. Despite the slightly different period, the error trend in the monthly 50th percentile (1985–2008) is remarkably similar to the H_s^{ANA} trend (1979–2012) presented here (see Fig. 5e). Even though the error trends were found to be mainly nonsignificant, they still suggest that trends obtained with H_s^{ANA} are enhanced by inhomogeneities, and that trends obtained with H_s^{FC48} offer a better estimate, as they are generally damped. When doing the same comparison based on the error trend in U_{10}^{ANA}, we cannot draw the same conclusion.

We have also compared trends in U_{10} and H_s with the results presented in Young et al. (2011) over corresponding periods (not shown). For mean U_{10} (comparable with Fig. 5d), we find the results very similar in the tropical Pacific. However, we find a stronger negative trend in the North Pacific and North Atlantic, more in favor of the NCEP–NCAR estimates presented in the supporting online material (SOM) of Young et al. (2011). For the SH, our estimates are far more moderate and less significant. In general, the ERA-I U_{10} trends are statistically significant for a smaller fraction of the global marine surface. For H_s (comparable with Fig. 6c), both studies find negative trends in the North Pacific and northeastern Atlantic. The biggest deviation is found in tropical areas where our estimates are more positive and significant. In terms of extreme conditions, the two studies are not strictly comparable (e.g., monthly maxima herein versus 99th percentile). Even so, it should be noted that our study does not underpin an increase in extreme H_s and U_{10} on higher latitudes ($>20°$N/S). This result might be influenced by the fact that ERA-I underestimates the upper percentiles (Stopa and Cheung 2014).

6. Concluding remarks

In this study we illustrate how the implementation of wave altimeter assimilation in August 1991 imposes a step change in the ERA-I wave statistics, affecting trends. We find that areas with higher model bias like the northeastern Atlantic and the eastern tropical Pacific are especially affected.

From two stand-alone wave model runs with and without wave altimeter assimilation (over the period 1992–2011) we show that different satellite updates, the number of operating satellites and the availability of wave altimeter data affect wave statistics and trends. Still, these effects are minor in most areas, compared to the sudden introduction of altimeter wave heights in August 1991.

For wind speed, no major step changes are detected. We do however find that the wind speed from analysis is increasing relative to the wind speed at increased forecast range up until about 2005. We cannot conclude whether this is an effect of assimilation alone, a real trend, or a combination of the two. Based on the fact that changes in wind speed at the time of analysis can be associated with assimilation updates, as seen with QuikSCAT in the Southern Hemisphere in 2000, we find it highly likely that trends in wind speed also are affected by assimilation.

Trends in wind speed and wave height seem to be damped or slightly shifted toward the negative using

data at increased forecast range. Still, we find that the 10-day forecast is capable of representing the main spatial features of the trend found at analysis. Here, we recommend using FC48 for trend analysis, as we do not want to completely remove the positive impact of assimilation. In swell-dominated areas (e.g., the eastern equatorial Pacific), one might even go to FC72 or more, as these areas in many cases are affected by assimilation more than three days ahead.

Based on ERA-I at the 48-h forecast range we find the following annual trends over the period 1979–2012; no trend or a slightly negative trend in mean wind and wave conditions in the northern parts of the Pacific and Atlantic Oceans, and positive trends in mean conditions in the tropical ocean areas, especially in wind speed in the western part of the equatorial Pacific by $>0.5\%$ yr^{-1}, an approximately 20% increase over the 34 years. In the Southern Hemisphere, the South Pacific stands out as the area with markedly increasing trends. In terms of maximum conditions, trends behave fairly similar to its mean counterpart. In general, trends in wind speed are more geographically confined, while trends in wave height are more spread out. Given the ability of waves to propagate over vast distances, this comes as no surprise. Overall, we find that global trends in wave height are stronger than corresponding wind estimates based on integrated mean and maximum conditions.

REFERENCES

Aarnes, O. J., O. Breivik, and M. Reistad, 2012: Wave extremes in the northeast Atlantic. *J. Climate,* **25,** 1529–1543, doi:10.1175/JCLI-D-11-00132.1.

Abdalla, S., 2012: Ku-band radar altimeter surface wind speed algorithm. *Mar. Geod.,* **35** (supplement 1), 276–298, doi:10.1080/01490419.2012.718676.

——, P. A. Janssen, and J.-R. Bidlot, 2011: Altimeter near real time wind and wave products: Random error estimation. *Mar. Geod.,* **34,** 393–406, doi:10.1080/01490419.2011.585113.

Appendini, C. M., A. Torres-Freyermuth, P. Salles, J. López-González, and E. T. Mendoza, 2014: Wave climate and trends for the Gulf of Mexico: A 30-yr wave hindcast. *J. Climate,* **27,** 1619–1632, doi:10.1175/JCLI-D-13-00206.1.

Bengtsson, L., K. I. Hodges, and E. Roeckner, 2006: Storm tracks and climate change. *J. Climate,* **19,** 3518–3543, doi:10.1175/JCLI3815.1.

Bertin, X., E. Prouteau, and C. Letetrel, 2013: A significant increase in wave height in the North Atlantic Ocean over the 20th century. *Global Planet. Change,* **106,** 77–83, doi:10.1016/j.gloplacha.2013.03.009.

Bidlot, J.-R., D. J. Holmes, P. A. Wittmann, R. Lalbeharry, and H. S. Chen, 2002: Intercomparison of the performance of operational ocean wave forecasting systems with buoy data. *Wea. Forecasting,* **17,** 287–310, doi:10.1175/1520-0434(2002)017<0287:IOTPOO>2.0.CO;2.

Boisséson, E., M. Balmaseda, S. Abdalla, E. Källén, and P. Janssen, 2014: How robust is the recent strengthening of the tropical Pacific trade winds? *Geophys. Res. Lett.,* **41,** 4398–4405, doi:10.1002/2014GL060257.

Breivik, Ø., O. J. Aarnes, J.-R. Bidlot, A. Carrasco, and Ø. Saetra, 2013: Wave extremes in the northeast Atlantic from ensemble forecasts. *J. Climate,* **26,** 7525–7540, doi:10.1175/JCLI-D-12-00738.1.

——, ——, S. Abdalla, J.-R. Bidlot, and P. A. Janssen, 2014: Wind and wave extremes over the world oceans from very large ensembles. *Geophys. Res. Lett.,* **41,** 5122–5131, doi:10.1002/2014GL060997.

Bromirski, P. D., D. R. Cayan, J. Helly, and P. Wittmann, 2013: Wave power variability and trends across the North Pacific. *J. Geophys. Res. Oceans,* **118,** 6329–6348, doi:10.1002/2013JC009189.

Caires, S., and A. Sterl, 2005: 100-year return value estimates for ocean wind speed and significant wave height from the ERA-40 data. *J. Climate,* **18,** 1032–1048, doi:10.1175/JCLI-3312.1.

Cavaleri, L., B. Fox-Kemper, and M. Hemer, 2012: Wind waves in the coupled climate system. *Bull. Amer. Meteor. Soc.,* **93,** 1651–1661, doi:10.1175/BAMS-D-11-00170.1.

Dee, D., and Coauthors, 2011: The ERA-Interim reanalysis: Configuration and performance of the data assimilation system. *Quart. J. Roy. Meteor. Soc.,* **137,** 553–597, doi:10.1002/qj.828.

Dietz, E. J., and T. J. Killeen, 1981: A nonparametric multivariate test for monotone trend with pharmaceutical applications. *J. Amer. Stat. Assoc.,* **76,** 169–174, doi:10.1080/01621459.1981.10477624.

Dobrynin, M., J. Murawsky, and S. Yang, 2012: Evolution of the global wind wave climate in CMIP5 experiments. *Geophys. Res. Lett.,* **39,** L18606, doi:10.1029/2012GL052843.

Dodet, G., X. Bertin, and R. Taborda, 2010: Wave climate variability in the north-east Atlantic Ocean over the last six decades. *Ocean Modell.,* **31,** 120–131, doi:10.1016/j.ocemod.2009.10.010.

Dragani, R., S. Abdalla, R. Engelen, A. Inness, and J.-N. Thépaut, 2015: Ten years of ENVISAT observations at ECMWF: A review of activities and lessons learnt. *Quart. J. Roy. Meteor. Soc.,* doi:10.1002/qj.2380, in press.

Gemmrich, J., B. Thomas, and R. Bouchard, 2011: Observational changes and trends in northeast Pacific wave records. *Geophys. Res. Lett.,* **38,** L22601, doi:10.1029/2011GL049518.

Gibson, J., P. Kallberg, S. Uppala, A. Hernandez, A. Nomura, and E. Serrano, 1997: ERA description. ECMWF Rep. Series 1, 71 pp.

Hanley, K. E., S. E. Belcher, and P. P. Sullivan, 2010: A global climatology of wind–wave interaction. *J. Phys. Oceanogr.,* **40,** 1263–1282, doi:10.1175/2010JPO4377.1.

Hemer, M. A., J. A. Church, and J. R. Hunter, 2010: Variability and trends in the directional wave climate of the Southern Hemisphere. *Int. J. Climatol.,* **30,** 475–491, doi:10.1002/joc.1900.

——, Y. Fan, N. Mori, A. Semedo, and X. L. Wang, 2013: Projected changes in wave climate from a multi-model ensemble. *Nat. Climate Change,* **3,** 471–476, doi:10.1038/nclimate1791.

Hirsch, R. M., and J. R. Slack, 1984: A nonparametric trend test for seasonal data with serial dependence. *Water Resour. Res.,* **20,** 727–732, doi:10.1029/WR020i006p00727.

——, ——, and R. A. Smith, 1982: Techniques of trend analysis for monthly water quality data. *Water Resour. Res.,* **18,** 107–121, doi:10.1029/WR018i001p00107.

Hodges, K., R. Lee, and L. Bengtsson, 2011: A comparison of extratropical cyclones in recent reanalyses ERA-Interim, NASA MERRA, NCEP CFSR, and JRA-25. *J. Climate,* **24,** 4888–4906, doi:10.1175/2011JCLI4097.1.

Hurrell, J. W., 1995: Decadal trends in the North Atlantic oscillation. *Science,* **269,** 676–679, doi:10.1126/science.269.5224.676.

Izaguirre, C., F. J. Méndez, A. Espejo, I. J. Losada, and B. G. Reguero, 2013: Extreme wave climate changes in Central-South America. *Climatic Change,* **119,** 277–290, doi:10.1007/s10584-013-0712-9.

Janssen, P., 2004: *The Interaction of Ocean Waves and Wind.* Cambridge University Press, 300 pp.

Kendall, M. G., 1948: *Rank Correlation Methods.* Griffin, 160 pp.

Khon, V., I. Mokhov, F. Pogarskiy, A. Babanin, K. Dethloff, A. Rinke, and H. Matthes, 2014: Wave heights in the 21st century Arctic Ocean simulated with a regional climate model. *Geophys. Res. Lett.,* **41,** 2956–2961, doi:10.1002/2014GL059847.

Lionello, P., H. Günther, and P. A. Janssen, 1992: Assimilation of altimeter data in a global third-generation wave model. *J. Geophys. Res.,* **97,** 14 453–14 474, doi:10.1029/92JC01055.

Mann, H. B., 1945: Nonparametric test against trend. *Econometrika,* **13,** 245–259. [Available online at http://www.jstor.org/stable/1907187.]

Reguero, B., F. Méndez, and I. Losada, 2013: Variability of multivariate wave climate in Latin America and the Caribbean. *Global Planet. Change,* **100,** 70–84, doi:10.1016/j.gloplacha.2012.09.005.

Semedo, A., K. Sušelj, A. Rutgersson, and A. Sterl, 2011: A global view on the wind sea and swell climate and variability from ERA-40. *J. Climate,* **24,** 1461–1479, doi:10.1175/2010JCLI3718.1.

Sen, P. K., 1968: Estimates of the regression coefficient based on Kendall's tau. *J. Amer. Stat. Assoc.,* **63,** 1379–1389, doi:10.1080/01621459.1968.10480934.

Simmons, A., P. Poli, D. Dee, P. Berrisford, H. Hersbach, S. Kobayashi, and C. Peubey, 2014: Estimating low-frequency variability and trends in atmospheric temperature using ERA-Interim. *Quart. J. Roy. Meteor. Soc.,* **140,** 329–353, doi:10.1002/qj.2317.

Sterl, A., and S. Caires, 2005: Climatology, variability and extrema of ocean waves: The Web-based KNMI/ERA-40 wave atlas. *Int. J. Climatol.,* **25,** 963–977, doi:10.1002/joc.1175.

——, and Coauthors, 2012: A look at the ocean in the EC-Earth climate model. *Climate Dyn.,* **39,** 2631–2657, doi:10.1007/s00382-011-1239-2.

Stopa, J. E., and K. F. Cheung, 2014: Intercomparison of wind and wave data from the ECMWF Reanalysis Interim and the NCEP Climate Forecast System Reanalysis. *Ocean Modell.,* **75,** 65–83, doi:10.1016/j.ocemod.2013.12.006.

——, ——, H. L. Tolman, and A. Chawla, 2013: Patterns and cycles in the climate forecast system reanalysis wind and wave data. *Ocean Modell.,* **70,** 207–220, doi:10.1016/j.ocemod.2012.10.005.

Ulbrich, U., G. Leckebusch, and J. Pinto, 2009: Extra-tropical cyclones in the present and future climate: A review. *Theor. Appl. Climatol.,* **96,** 117–131, doi:10.1007/s00704-008-0083-8.

Uppala, S. M., and Coauthors, 2005: The ERA-40 Re-Analysis. *Quart. J. Roy. Meteor. Soc.,* **131,** 2961–3012, doi:10.1256/qj.04.176.

Vincent, L. A., X. L. Wang, E. J. Milewska, H. Wan, F. Yang, and V. Swail, 2012: A second generation of homogenized Canadian monthly surface air temperature for climate trend analysis. *J. Geophys. Res.,* **117,** D18110, doi:10.1029/2012JD017859.

Wan, H., X. L. Wang, and V. R. Swail, 2010: Homogenization and trend analysis of Canadian near-surface wind speeds. *J. Climate,* **23,** 1209–1225, doi:10.1175/2009JCLI3200.1.

Wang, X. L., 2008a: Accounting for autocorrelation in detecting mean shifts in climate data series using the penalized maximal t or F test. *J. Appl. Meteor. Climatol.,* **47,** 2423–2444, doi:10.1175/2008JAMC1741.1.

——, 2008b: Penalized maximal F test for detecting undocumented mean shift without trend change. *J. Atmos. Oceanic Technol.,* **25,** 368–384, doi:10.1175/2007JTECHA982.1.

——, and V. R. Swail, 2001: Changes of extreme wave heights in Northern Hemisphere oceans and related atmospheric circulation regimes. *J. Climate,* **14,** 2204–2221, doi:10.1175/1520-0442(2001)014<2204:COEWHI>2.0.CO;2.

——, and ——, 2002: Trends of Atlantic wave extremes as simulated in a 40-yr wave hindcast using kinematically reanalyzed wind fields. *J. Climate,* **15,** 1020–1035, doi:10.1175/1520-0442(2002)015<1020:TOAWEA>2.0.CO;2.

——, and Y. Feng, 2013: RHtestsV4 User Manual. Climate Research Division, ASTD, STB, Environment Canada, 28 pp. [Available online at http://etccdi.pacificclimate.org/software.shtml.]

——, Q. H. Wen, and Y. Wu, 2007: Penalized maximal t test for detecting undocumented mean change in climate data series. *J. Appl. Meteor. Climatol.,* **46,** 916–931, doi:10.1175/JAM2504.1.

——, H. Chen, Y. Wu, Y. Feng, and Q. Pu, 2010: New techniques for the detection and adjustment of shifts in daily precipitation data series. *J. Appl. Meteor. Climatol.,* **49,** 2416–2436, doi:10.1175/2010JAMC2376.1.

——, Y. Feng, and V. Swail, 2012: North Atlantic wave height trends as reconstructed from the 20th century reanalysis. *Geophys. Res. Lett.,* **39,** L18705, doi:10.1029/2012GL053381.

Young, I., S. Zieger, and A. Babanin, 2011: Global trends in wind speed and wave height. *Science,* **332,** 451–455, doi:10.1126/science.1197219.

——, J. Vinoth, S. Zieger, and A. Babanin, 2012: Investigation of trends in extreme value wave height and wind speed. *J. Geophys. Res.,* **117,** C00J06, doi:10.1029/2011JC007753.

Yue, S., P. Pilon, and G. Cavadias, 2002: Power of the Mann–Kendall and Spearman's rho tests for detecting monotonic trends in hydrological series. *J. Hydrol.,* **259,** 254–271, doi:10.1016/S0022-1694(01)00594-7.